LA-10561-MS

549

By exc
SAI
T&MSS
LIBRARY

Los Alamos National Laboratory is operated by the University of California for the United States Department of Energy under contract W-7405-ENG-36.

Los Alamos
Los Alamos National Laboratory
Los Alamos, New Mexico 87545

An Affirmative Action/Equal Opportunity Employer

Prepared by Nevada Nuclear Waste Storage Investigations (NNWSI) Project participants as part of the Civilian Radioactive Waste Management Program. The NNWSI Project is managed by the Waste Management Project Office of the US Department of Energy, Nevada Operations Office. NNWSI Project work is sponsored by the Office of Geologic Repositories of the DOE Office of Civilian Radioactive Waste Management.

DISCLAIMER

This report was prepared as an account of work sponsored by an agency of the United States Government. Neither the United States Government nor any agency thereof, nor any of their employees, makes any warranty, express or implied, or assumes any legal liability or responsibility for the accuracy, completeness, or usefulness of any information, apparatus, product, or process disclosed, or represents that its use would not infringe privately owned rights. Reference herein to any specific commercial product, process, or service by trade name, trademark, manufacturer, or otherwise, does not necessarily constitute or imply its endorsement, recommendation, or favoring by the United States Government or any agency thereof. The views and opinions of authors expressed herein do not necessarily state or reflect those of the United States Government or any agency thereof.

LA-10561-MS

UC-70
Issued: December 1985

Petrochemical Variation of Topopah Spring Tuff Matrix with Depth (Stratigraphic Level), Drill Hole USW G-4, Yucca Mountain, Nevada

F. M. Byers, Jr.

SAI
T&MSS
LIBRARY

Los Alamos
Los Alamos National Laboratory
Los Alamos, New Mexico 87545

CONTENTS

ABSTRACT 1

I. INTRODUCTION 1
A. Scope and Purpose of Report 1
B. Geologic Setting 2
C. Previous Work on the Topopah Spring Member 4

II. APPROACH AND METHODS 5
A. Categories of Matrix Textures 5
B. Thin Section Modal Analysis 8
C. Microprobe Analysis of Groundmass 10

III. RESULTS 11
A. Petrographic Variation of Matrix with Depth 11
B. Chemical Variation of Glassy and Cryptocrystalline Groundmass 15

IV. DISCUSSION AND CONCLUSIONS 18
A. Relation of Textures to Emplacement History 18
B. Use of Textures to Guide Drilling in Exploratory Shaft . 20

ACKNOWLEDGMENTS 22

REFERENCES 23

APPENDIX A PETROGRAPHIC MODAL DATA FOR THIN SECTIONS OF TOPOPAH SPRING MEMBER, USW G-4, YUCCA MOUNTAIN, NEVADA 27

APPENDIX B ELECTRON MICROPROBE ANALYSES OF GROUNDMASSES, TOPOPAH SPRING MEMBER, USW G-4, YUCCA MOUNTAIN, NEVADA 31

PETROCHEMICAL VARIATION OF TOPOPAH SPRING TUFF MATRIX WITH DEPTH (STRATIGRAPHIC LEVEL), DRILL HOLE USW G-4, YUCCA MOUNTAIN, NEVADA

by

F. M. Byers, Jr.

ABSTRACT

This study describes and interprets petrochemical variation of the matrix (excluding fractures and large gas cavities) of the Topopah Spring Member of the Paintbrush Tuff. This tuff includes the candidate host rock for a high-level nuclear waste repository at Yucca Mountain on the Nevada Test Site. Cored hole USW G-4, near the site of a potential exploratory shaft at Yucca Mountain, penetrated 359.4 m (1179 ft) of the member within the unsaturated zone. This study shows that petrographic textures and chemistry of the matrix vary systematically within recognizable lithologic subunits related to crystallization (cooling) zones, welding (compaction) zones, and compositional zones (rhyolite versus quartz latite). The methods used for this study include petrographic modal thin section analysis using an automated counter and electron microprobe analysis of the groundmass. Distinctive textural categories are defined, and they can be ranked from finest to coarsest as vitrophyre (glass), cryptocrystalline groundmass, spherulites, granophyre, lithic fragments, and phenocrysts. The two main groundmass compositions are also defined: rhyolite (high silica) and quartz latite. The value of these petrochemical studies lies in providing microscopic criteria for recognizing the zonal subunits where they may have greatly limited exposure, as in mined drifts and in core from horizontal drill holes. For example, the lower nonlithophysal zone can be distinguished microscopically from the middle nonlithophysal zone by (1) degree of compaction, (2) amount of quartz, and (3) amount of lithic fragments. The variability between these textural categories should also be considered in designing physical and chemical tests of the Topopah Spring.

I. INTRODUCTION

A. Scope and Purpose of Report

Yucca Mountain in the southwestern part of the Nevada Test Site is one of three candidate sites recommended in December 1984 by the Secretary of Energy for a national nuclear waste repository, as required by the Nuclear Waste

Policy Act of 1982 (Public Law 97-425, January 7, 1983). Yucca Mountain is underlain by a thick sequence of tuffs cut by several fault zones (Scott and Bonk 1984). The Topopah Spring Member of the Paintbrush Tuff was selected in mid-1982 as a candidate rock unit for an underground mined repository because this welded tuff member is slightly over 1000 ft thick in the least faulted area, the Yucca Mountain Exploration Block (Fig. 1), and has thermal properties similar to granitic rocks. On the average the base of the Topopah Spring tuff is about 1400 ft below the surface, and the tuff occurs entirely in the unsaturated zone within the Exploration Block. Studies at Yucca Mountain are directed by the Nevada Nuclear Waste Storage Investigations (NNWSI) project, which is managed by the Nevada Operations Office of the U.S. Department of Energy.

This report describes petrographic and petrochemical studies related to depth (stratigraphic position) within the Topopah Spring Member based on thin sections (slides) of drill core USW G-4, approximately 91.4 m (300 ft) S30°W of the potential location of the Yucca Mountain Exploratory Shaft (ES). These petrographic studies relate to and provide background for detailed tests for site characterization described in the Exploratory Shaft Test Plan (ESTP) (C. W. Myers et al. November 28, 1983). The Topopah Spring Member is not a homogeneous welded tuff but has vertical zones of primary composition, welding, and texture (Smith 1960; Lipman et al. 1966), which are genetically related to three major eruptive pulses at the time of emplacement. Although this vertical zonation is easily recognizable in cored drill holes and outcrop, studies of matrix petrography in thin sections of the different zones discussed in this report add additional refinement to the site characterization. Such studies might also provide a data base for resolving an unforeseen engineering problem under Yucca Mountain at some future date. For example, this study should aid in determining stratigraphic position within the Topopah Spring during sinking of the proposed ES and during underground drifting and horizontal drilling either from the ES or during repository construction. The petrographic variation of the matrix may prove especially helpful in determining stratigraphic position on the far side of subsurface faults encountered during drifting or drilling.

B. Geologic Setting

The Topopah Spring Member as penetrated in drill hole USW G-4 is described by Spengler and Chornack (1984). Their stratigraphic subdivisions,

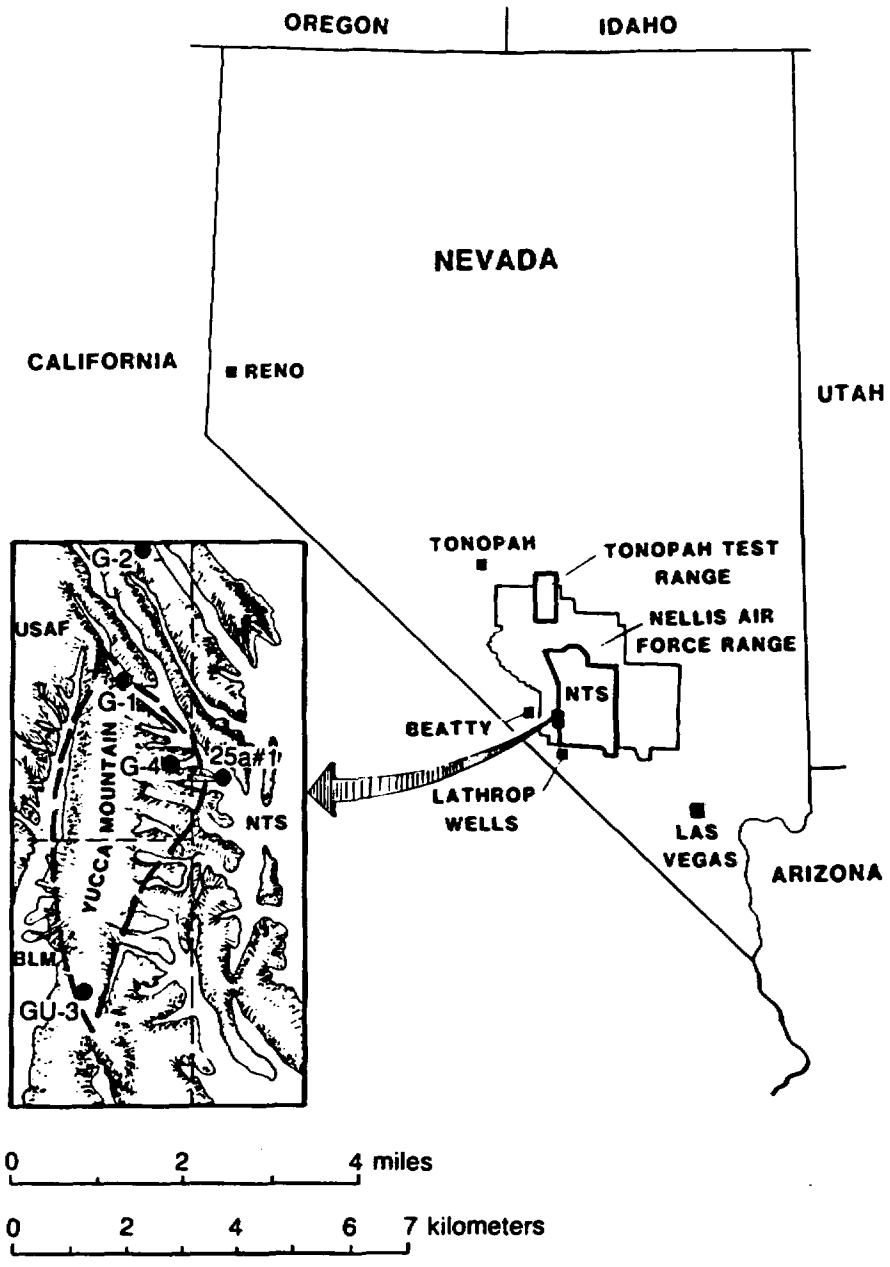

Fig. 1.
Index map of the Yucca Mountain area, Nevada, showing location of drill hole USW G-4, other continuously cored holes, and the outline of the Yucca Mountain Exploration Block. (NTS) Nevada Test Site, (USAF) U.S. Air Force buffer zone, (BLM) Bureau of Land Management exploration lease.

shown in the columnar section at the left side of Fig. 2 (in pocket), form the geologic setting of this report. The Topopah Spring is moderately to densely welded throughout except for thin non- to partially welded zones in uppermost and lowermost parts. The lithologic column penetrated in USW G-4 is similar to those penetrated in USW G-1 (Spengler et al. 1981), USW GU-3 (Scott and Castellanos 1984), and UE-25a#1 (Spengler et al. 1979), but it differs somewhat from that in USW G-2 (Maldonado and Koether 1983). Noteworthy is the fact that the Topopah Spring exposed in outcrop (author's unpublished data), just east of the area shown in Fig. 1, contains the same zones as those penetrated in drill holes in the Yucca Mountain Repository Block, although the outcrop zones are only about half as thick. The variation of the matrix petrography between USW G-4 and other cored holes at Yucca Mountain will be the subject of a later report.

C. Previous Work on the Topopah Spring Member

The stratigraphy and petrology of the Topopah Spring Member were first formally treated by Lipman et al. (1966), who described the welding, crystallization, and primary compositional zonation from measured and sampled outcrops in the vicinity of Yucca Mountain. These authors recognized the distinctive upper lithophysal zone (Fig. 2), which they called the "main lithophysal zone," as well as the obvious lower and upper vitrophyres. The microcrystalline (devitrified) tuff, including the "candidate host rock" (C. W. Myers et al. 1983) between the lower vitrophyre and the upper lithophysal zone, was recognized as having "several thin vapor-phase and lithophysal zones. . . within it" (Lipman et al. 1966, p. F5), but the lower lithophysal zone was not recognized as such by Lipman et al., owing to limited exposures. Their paper also deals with the primary compositional zonation as it relates to the chemistry of the magma chamber in the source vent area, more recently considered to be the Claim Canyon cauldron north of Yucca Mountain (Byers et al. 1976b). The primary compositional zonation, manifested principally by vertical changes in groundmass chemistry, phenocryst abundance, and phenocryst assemblage, is also the subject of this report.

II. APPROACH AND METHODS

A. Categories of Matrix Textures

The matrix of the Topopah Spring is defined herein as the major bulk of the unit, exclusive of open fractures, of fracture fillings larger than about

200 μm (0.2 mm), and of lithophysal cavities and xenoliths larger than about 5 mm. This is a practical definition based on statistical considerations related to the small area (20 x 30 mm) of thin sections. These thin sections may cut sparse veinlets less than 200 μm wide, and in the upper lithophysal zone (Fig. 2), it is difficult, if not impossible, to avoid intersecting small lithophysal cavities with diameters of 5 mm or less. The microveinlets observed in slides, however, are almost always filled with silica minerals and alkali feldspar, and they commonly connect with those in the lithophysal cavity linings and in the flattened granophyric cores of former pumice (Carlos 1985). Granophyric pumice is a significant matrix category because of the larger size of its crystals (up to 0.5 mm) and because the crystals commonly line cavities in the interiors of pumice. In several drill holes microscopic heulandite and rare mordenite (Bish et al. 1981; Caporuscio et al. 1982; Spengler et al. 1981) also occur in the centers of microveinlets and in granophyric pumice within a few tens of feet above the lower vitrophyre. Fortunately for statistical analysis, the thin sections from the USW G-4 site used in this study were cut with no separate element of the matrix having an average diameter larger than about 5 mm.

The elongate bar graphs in the central part of Fig. 2 compare coarse to fine textures between the different stratigraphic levels, starting with coarsest (crystals and lithic fragments) at the left and ranging to finest (cryptocrystalline, glass, and voids) at the right. Phenocrysts and lithic fragments are generally the coarsest, ranging from 0.1 mm to about 2.0 mm for phenocrysts and as much as 5 mm for lithics. The granophyric intergrowths (alkali feldspar and silica minerals, Fig. 3a) and silica-filled microvesicles (cristobalite and/or tridymite, Fig. 3b) both range from approximately 0.05 mm to approximately 0.5 mm and are most abundant in the lithophysal zones. Feldspar-silica intergrowths with individual crystals smaller than about 0.05 mm produce a microlitic or spherulitic aggregate (Figs. 4a, 4b) in which it is difficult or impossible to identify individual minerals; however, spherulitic crystals are elongate, radiate from a common center, and rarely attain several millimeters in length. Nearly all spherulite crystals in the Topopah Spring matrix are less than 0.5 mm in length and 0.05 mm in width. A smaller grain-size aggregate (individual crystals less than about 0.005 mm) is called cryptocrystalline (Figs. 4a, 4b, and 5a) because the individual crystals cannot be distinguished even at 200X; x-ray diffraction studies indicate that

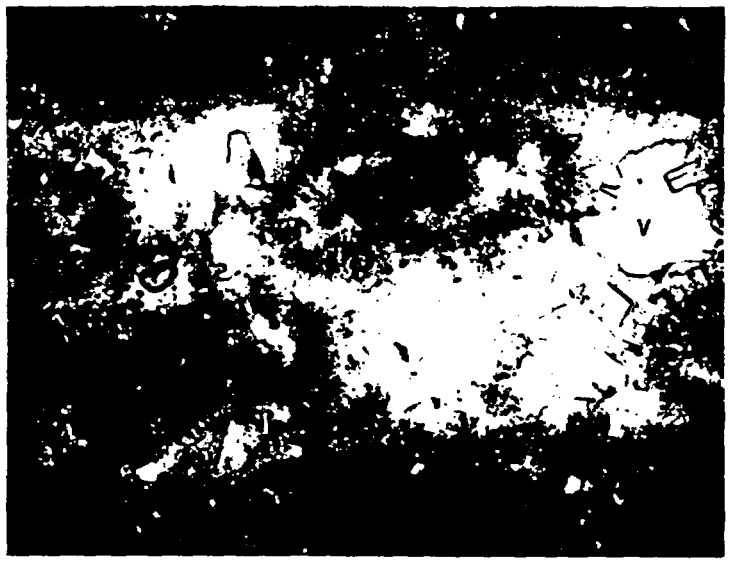

(a)

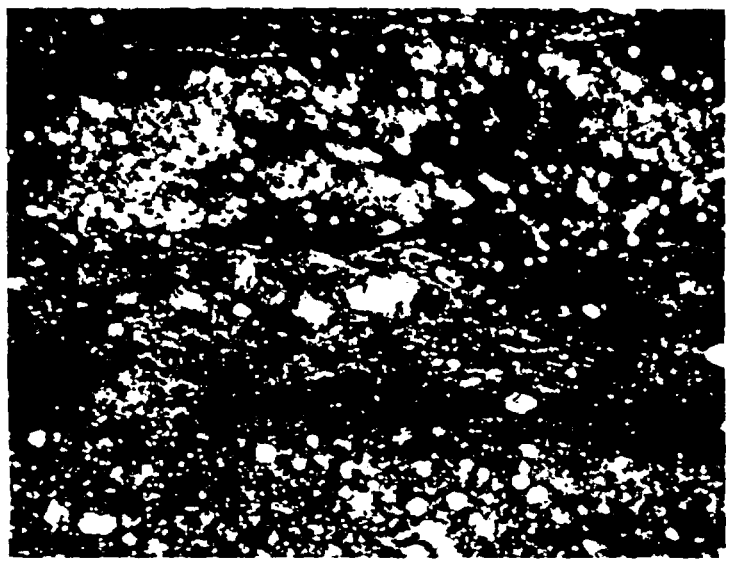

(b)

Fig. 3.
(a) Granophyric intergrowth of quartz and alkali feldspar (dark, rectangular outlines) in the central part of former pumice; (v) void. Granophyric texture enclosed by coarse spherulites, some of which have voids at the center. Depth 249.0 m (817 ft). Lower lithophysal zone. Long dimension of the photograph is 3 mm; plane polarized light.
(b) Densely welded tuff at 284.7 m (934 ft), showing different sizes of cristobalite/tridymite-filled vesicles (amygdules), concentrated mainly in flattened pumice of lower lithophysal zone. Groundmass is entirely microlitic/spherulitic, leaving only "ghosts" of flattened former shards between pumices. Long dimension of the photograph is 3 mm; plane polarized light.

(a)

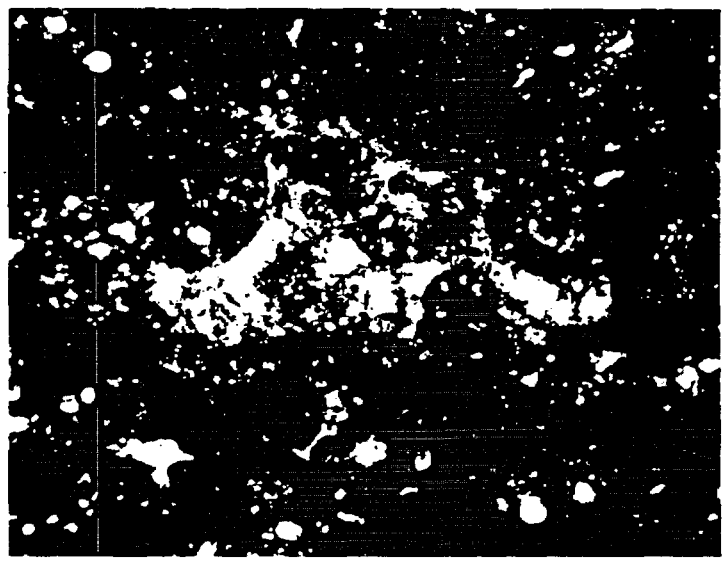

(b)

Fig. 4.
(a) Densely welded tuff at 379.2-m (1244-ft) depth, lower nonlithophysal zone. Flattened and elongated former shards and small pumice. Shards are cryptocrystalline, but pumice is microlitic to spherulitic with granophyric interiors of silica minerals and alkali feldspars. Long dimension of the photograph is 3 mm; plane polarized light.
(b) Densely welded tuff at 227.4-m (746-ft) depth, middle nonlithophysal zone. Spherulitic former pumice enclosed by cryptocrystalline groundmass showing light-transmissive shard walls. Compare with 379.2 m (1244 ft) in lower nonlithophysal zone. The cryptocrystalline groundmass with relict shard texture may have initially chilled to a glass but later devitrified during the slow cooling of the Topopah Spring Member interior. Long dimension of the photograph is 3 mm; plane polarized light.

in addition to alkali feldspars and silica minerals the cryptocrystalline aggregate may include smectite and other hydrated secondary minerals above the basal vitrophyre (Levy 1984a, p. 27-30; 1984b, p. 36; 1985, p. 366). As seen in thin section, the cryptocrystalline aggregates are semitranslucent to nearly opaque. The cryptocrystalline aggregates may grade into a glassy groundmass or into vitrophyre (Fig. 5b).

B. Thin Section Modal Analysis

Polished thin sections were made from 22 samples of USW G-4 drill core at the thin section laboratory in Area TA-33, Los Alamos, for modal analysis and for analysis by electron microprobe. These standard sections, 0.03 mm thick, were mounted on glass slides and polished. In this report, thin sections are referred to as slides for brevity.

The Los Alamos suite of 22 slides of the Topopah Spring Member was supplemented by 3 conventional slides (with cover glasses) from the USGS. All slides were point counted at 200X magnification using an automated electric point counter. For point counting the matrix, 20 to 22 traverses 28.2 mm long and spaced 1.0 mm apart were made across the slide at 0.105-mm point count intervals. This combination of traverses and point intervals generally yielded 5000-6000 points per slide, depending on the size and geometry of the slide, and was adequate to determine volume percentages of texture types, lithics, and total phenocrysts in any given slide (Fig. 2; Appendix A, Table A-I).

Slides prepared from adjacent samples within 0.3 m (1 ft) of each other in Yucca Mountain drill cores may commonly differ in minor textural constituents, owing to the small area (6 cm^2) sectioned. Minor constituents from two adjacent sections of core may differ as much as two sections 50 ft apart (vertically). Two closely spaced slides from USW G-4, a Los Alamos sample from 625 ft depth and a USGS sample from 625.7 ft depth, differ greatly in lithic content; this difference probably reflects sample error. The general petrographic trends in Fig. 2, however, are determined from many samples and are thus significant, and moreover they relate to the gross observable lithology as recorded by the USGS (Spengler and Chornack 1984).

The phenocryst proportions in percentages, shown in Fig. 2 and Appendix A, Table A-I, present a special statistical problem because the lower three-fourths of the Topopah Spring has only about 1% total phenocrysts. Therefore, a slide with 6 cm^2 surface area would contain only 6 mm^2 of

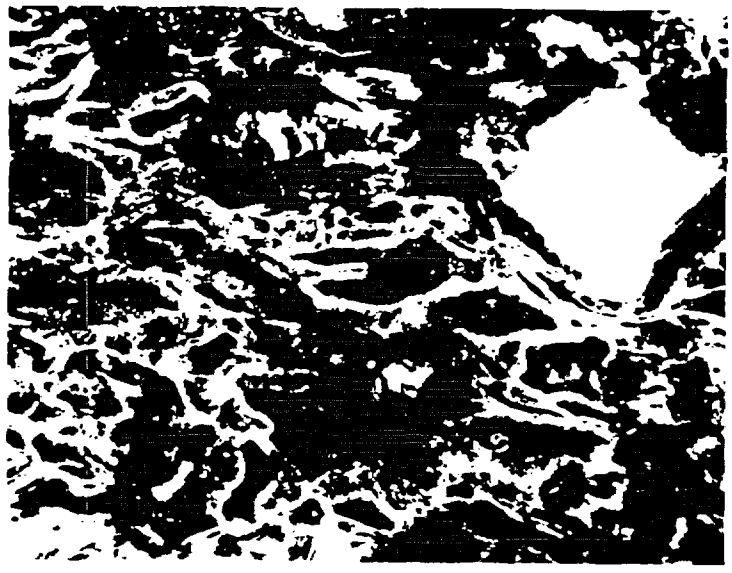

(a)

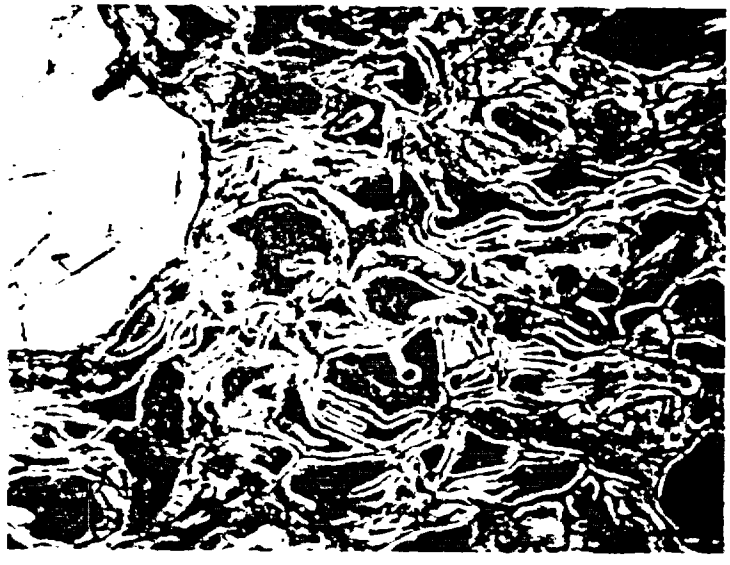

(b)

Fig. 5.
(a) Densely welded, incipiently devitrified cryptocrystalline tuff at 395.9-m (1299-ft) depth, lower nonlithophysal zone. Flattened former shards, probably once glassy, devitrified during cooling subsequent to emplacement but are still outlined by thin (±5-μm) colorless material, now very fine aggregate of silica minerals and alkali feldspars. Quartz phenocryst (xenocryst?) at right. Long dimension of the photograph is 1.2 mm; plane polarized light.
(b) Densely welded Topopah Spring lower vitrophyre at 405.7-m (1331-ft) depth. Flattened and elongated former shards outlined by thin (±5-μm) rim or wall of colorless glass. Compare colorless glass rims to rims of silica minerals and alkali feldspars in the photograph above. Quartz phenocryst (xenocryst?) at left. Long dimension of the photograph is 1.2 mm; plane polarized light.

phenocrysts. The quartz, feldspar, and mafic-accessory phenocryst of the Topopah Spring matrix vary with depth (stratigraphic position) in drill hole USW G-4, Yucca Mountain. Contacts in the stratigraphic column (Fig. 2) are from Spengler and Chornack 1984. Even with 6000 point counts per slide, only 60 and sometimes fewer counts fall on phenocrysts. With quartz and total mafic minerals, commonly amounting to only a few percentages of the total phenocrysts or a few hundredths of the total rock, more phenocryst points are needed even to semiquantitatively determine phenocryst proportions within an individual slide. (Replicate thin sections cut from adjacent core samples would doubtless show some improvement in statistics.) In order to reduce the counting error for the minerals visible in the slide, additional traverses were made between the original 1-mm traverses, resulting in an overall 1/2-mm traverse spacing. If core is sampled on the opposite (unknown) side of a fault, at least three slides should be prepared and counted in order to reduce the overall sample error.

C. Microprobe Analysis of Groundmass

Small areas within polished thin sections of the basal vitrophyre and cryptocrystalline groundmasses were analyzed for chemical composition by an automated Cameca electron microprobe, with accelerating potential set at 15 kV and a sample current of 15.5-nA on thorium oxide. In order to obtain a sufficiently large area of the section that was representative of cryptocrystalline groundmass, a 20-μm^2 (0.02 mm^2) raster was used, covering a surface area of 400 μm^2 (0.0004 mm^2). The 20-μm^2 raster is 4 times larger than the maximum linear grain size, 0.005 mm, and 16 times the area of the largest grain (0.0004 mm^2/0.000025 mm^2) in cryptocrystalline groundmass. Chemical compositions expressed as oxides were computer calculated from corrected peak intensities, using the Bence and Albee (1968) correction. Feldspar and amphibole standards were used for both the cryptocrystalline and the vitrophyre analyses. The microprobe analyses of cryptocrystalline groundmass, despite scatter, agree very well with those of the basal vitrophyre with a few exceptions to be discussed later. Also the microprobe analyses of the vitrophyre closely agree with those done by conventional wet analysis (Lipman et al. 1966, p. F33). The microprobe analyses of the cryptocrystalline groundmass and vitrophyre are at any rate internally consistent, and although they may be less accurate than other methods, they provide the only means of obtaining such small-scale analyses.

III. RESULTS

A. Petrographic Variation of Matrix with Depth

The internal stratigraphy of the Topopah Spring Member is divisible into three major subunits as a result of the petrographic studies of the matrix (Fig. 2). The lowest major subunit includes the basal vitrophyre, the lower nonlithophysal zone, and the overlying lower lithophysal zone. The middle major subunit contains the middle nonlithophysal zone and the overlying upper lithophysal zone (Fig. 6a). The upper subunit consists mainly of the crystal-rich vapor-phase zone, caprock, and upper vitrophyre. As can be seen in Fig. 2, the uppermost part of the middle subunit is gradational into the upper subunit by an upward increase in quartz latitic cryptocrystalline groundmass within the upper one-third of the upper lithophysal zone between 500 ft and upward to 400 ft (Fig. 6b). The minor amount of cryptocrystalline groundmass in slides from footages 556 and 514 is not quartz latitic; it is nearly opaque, and walls are relict shards like the opaque cryptocrystalline groundmass in slides at 1299 and 1282 ft.

The rhyolitic cryptocrystalline matrix of the middle nonlithophysal zone is similar in hand specimen to that of the lower nonlithophysal, but the matrices differ microscopically. Both exhibit textures of relict, formerly glassy shards, each of which is outlined by a wall, a few micrometers across, of darker cryptocrystalline material (Fig. 4). The middle lithophysal zone differs from the lower zone in being moderately welded with a pumice/shard flattening ratio of generally less than 4:1, whereas the lower zone has a ratio of more than 4:1 and therefore is densely welded. An interpretation of these and other variations will be given in the concluding section of this report.

Total phenocrysts (crystals) and lithic fragments also show variations with depth or stratigraphic position (Fig. 2; Appendix A, Table A-I). The percentage of phenocrysts in the lower rhyolitic three-fourths of the Topopah Spring ranges from 0.5 to 1.7%. This range is probably a between-sample error, owing to the restricted area of the slide (20 by 30 mm), rather than a counting error. However, the increase in phenocrysts in the upper one-fourth of the Topopah Spring is also associated with an increase in cryptocrystalline quartz latitic groundmass as originally pointed out by Lipman et al. (1966). The percentage of lithics below 1117 ft in the basal vitrophyre, lower nonlithophysal, and lowermost lower lithophysal varies from 1.2 to 3.2 and

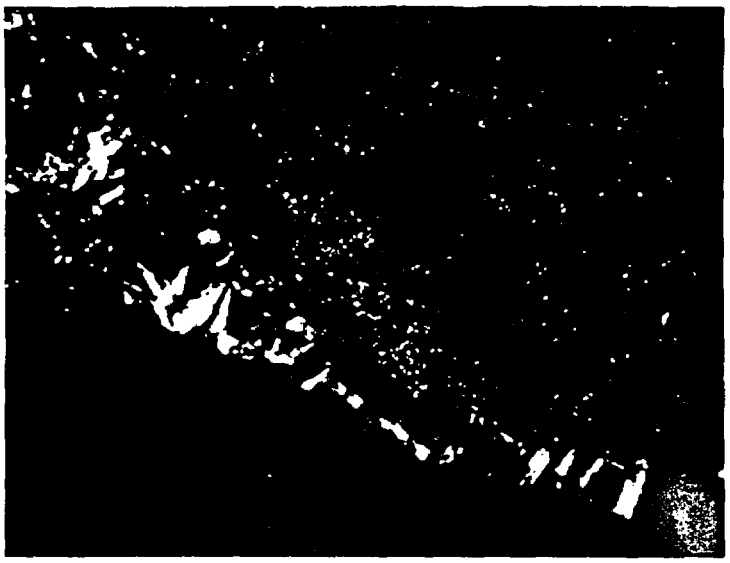

(a)

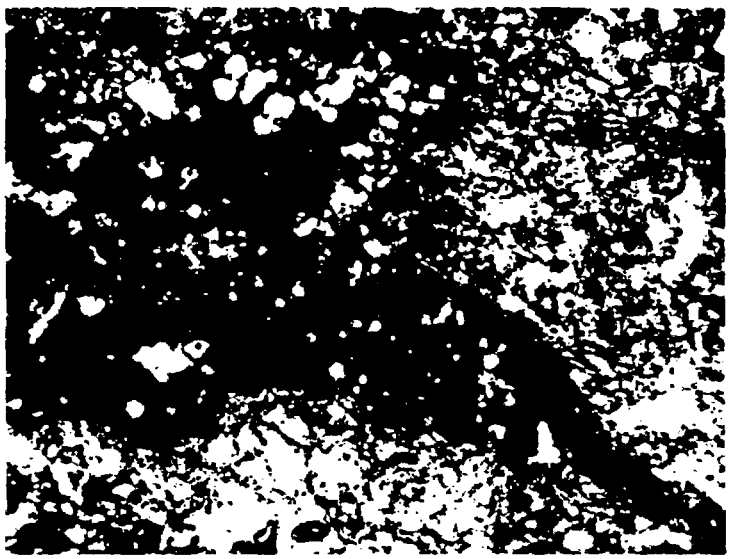

(b)

Fig. 6.
(a) Wedge-shaped tridymite lining lithophysal cavity at 169.5-m (556-ft) depth, upper lithophysal zone. Backing the tridymite lining are microlitic/spherulitic intergrowths with small cristobalite/tridymite-filled amygdules (barely visible). Long dimension, 3 mm; crossed nicols.
(b) Moderately welded devitrified tuff at 36.2-m (447-ft) depth; upper part of upper lithophysal zone. Quartz latite (dark) lenticle or shred (fiamma?) enclosed in rhyolitic microlitic groundmass. Light-transmissive small spheroidal/ellipsoidal areas are silica-filled vesicles (amygdules). Long dimension of the photograph is 3 mm; plane polarized light.

along with other criteria appears typical of the lower nonlithophysal. Upward, the percentage of lithic fragments is more erratic but in general decreases. In some thin sections taken within the nearly lithic-free middle part of the Topopah Spring, several examples have been observed of what once may have been former lithic fragments (a few have indistinct rhyolitic lava flow banding). These are now lenticular, parallel to the pumice foliation, and partially recrystallized to spherulites and granophyre.

Granophyre (Fig. 3a) and cristobalite/tridymite (SiO_2)-filled pores or vesicles (amygdules, Fig. 3b) occur in greatest abundance within the upper lithophysal zone (Fig. 2; Appendix A, Table A-I). The granophyre not only occurs within and/or lining lithophysal and pumice cavities but also may occur within vesicles, where it may consist largely of quartz. In some vesicles quartz and cristobalite and/or tridymite are present. Hence the categories of granophyre and amygdules (SiO_2-filled pores) are somewhat gradational in some slides sampled from the lithophysal zones. For that reason, the sum of the two categories is probably a safer criterion for identifying depth or stratigraphic position. However, it appears that in the upper two-thirds of the upper lithophysal, amygdules are significantly more abundant than in the lower one-third or in the lower lithophysal zone. Fortunately, another criterion is available; namely, cristobalite occurs dominantly in the vesicles within the lower lithophysal, whereas tridymite mainly fills the vesicles in the upper lithophysal (Fig. 6a), as reported by Bish et al. (1984).

Small voids or cavities within the thin section occur mainly within the upper lithophysal zone, where cutting a thin section is nearly impossible without cutting either small lithophysal cavities or pumice cavities. Two of the thin sections, taken at depths of 410 and 556 ft (Appendix A, Table A-I), were especially chosen because of the abundance of small lithophysal cavities and therefore may be somewhat biased for interpretation of matrix stratigraphy. However, except for the increased amount of tridymite-filled vesicles and decreased cryptocrystalline groundmass in the slide at 410 ft, the slide at 556 ft contains amounts of granophyre and vesicles similar to those in adjacent slides.

The proportions of quartz, sanidine, plagioclase, and total mafic minerals as percentages of total phenocrysts are given in Fig. 2 and Appendix A, Table A-I. Quartz is in general more abundant in the lower part of the Topopah Spring, but there is considerable overlap in the range of values

throughout the unit. By inspection of Fig. 2 and Appendix A, Table A-I, the rhyolitic portion can be subdivided by quartz phenocryst content into (1) the middle subunit defined by textures, (2) the lower lithophysal zone of the lower subunit, and (3) the lower nonlithophysal zone and basal vitrophyre of the lower subunit. The statistical parameters--arithmetic mean, standard deviation, and two standard errors of the mean for the percentage of quartz--are shown in Table I. The stratigraphically lowest subdivision, the vitrophyre and lower nonlithophysal, has a moderate percentage of quartz; the overlying lower lithophysal zone has a small amount; and the overlying middle nonlithophysal and upper lithophysal zones have a sparse amount. Standard deviations and two standard errors of the mean overlap among the three categories. These marginal statistical differences among zones are, however, corroborated by data for other cored holes on Yucca Mountain, which show the same general upward decrease in quartz.

The percentages of feldspar and mafic minerals vary more widely than do those of quartz. Therefore, they cannot be used to determine stratigraphic position within the rhyolitic lower three-quarters of the Topopah Spring. The sanidine/plagioclase ratio does, however, increase in the quartz latitic caprock, but this uppermost unit is easily recognized by other criteria.

TABLE I

STATISTICAL PARAMETERS FOR QUARTZ PHENOCRYSTS IN THE RHYOLITIC PORTION OF THE TOPOPAH SPRING
(Data in Appendix A, Table A-I)

Cooling Zones	No. Slides (n)	Arith. Mean ($\bar{X}$ in pct.)	Std. Dev. (s)	Two Std. Errors/Mean $2s_{\bar{X}}$
Upper lithophysal, middle nonlithophysal (middle subunit)	11	1.0	±2.0	±1.3
Lower lithophysal	5	4.8	±2.3	±2.3
Lower nonlithophysal, vitrophyre	6	11.3	±9.8	±8.8

B. Chemical Variation of Glassy and Cryptocrystalline Groundmasses

About 150 microprobe analyses (Figs. 7 and 8; Appendix B, Table B-I) were made in eight polished thin sections of glassy and cryptocrystalline groundmasses of the three major subunits. The three major subunits are the same as those defined by thin section modal analysis (Fig. 2): (1) the basal vitrophyre, the lower nonlithophysal zone above it, and the overlying lower lithophysal; (2) the middle nonlithophysal zone and the overlying upper lithophysal; and (3) the quartz latitic zone beginning at about 500 ft in the upper part of the upper lithophysal (Fig. 2) and culminating in the caprock vitrophyre. Only the glassy and cryptocrystalline groundmass of these subunits was analyzed by microprobe.

In the lowest fine-grained zone, microprobe analyses of glass in the basal vitrophyre (1331 ft) and of cryptocrystalline groundmasses in the overlying altered vitrophyre (1299 and 1282 ft) indicate similar high-silica rhyolitic compositions. The 13 probe analyses (10 of FeO) of the vitrophyre (Fig. 7; Appendix B, Table B-I) cluster well and show little dispersion. The values of the major oxides in the vitrophyre determined by microprobe also agree closely with those determined by conventional wet methods (Lipman et al. 1966, p. F33). The 10 analyses of FeO include 2 of clear glassy pumice and 8 of brown glass shards. Although based on only a few analyses, the iron content of the clear pumice glass is a few tenths of a percent lower than that in the brown glass shards, as observed in other analyses of the Topopah Spring vitrophyre (Levy 1984a). There is more dispersion of the probe analyses within the zone of altered vitrophyre, but the peaks or modes agree well with those of the vitrophyre except for potash. The peaks for potash are shifted about 1% higher in the cryptocrystalline groundmasses of the altered vitrophyre. However, several analyses are low in potash; these analyses were made on nearly opaque shard borders.

The microprobe analyses of cryptocrystalline groundmass of the middle nonlithophysal zone are represented by thin sections at 746 and 694 ft (Figs. 7 and 8). Both slides are high-silica rhyolite like that of the lower nonlithophysal zone, except there are no low potash analyses and no associated underlying altered vitrophyre.

The cryptocrystalline and glassy analyses of the upper quartz latitic subunit span four crystallization zones from the upper one-third of the upper lithophysal zone upward to the caprock vitrophyre. Three thin sections at

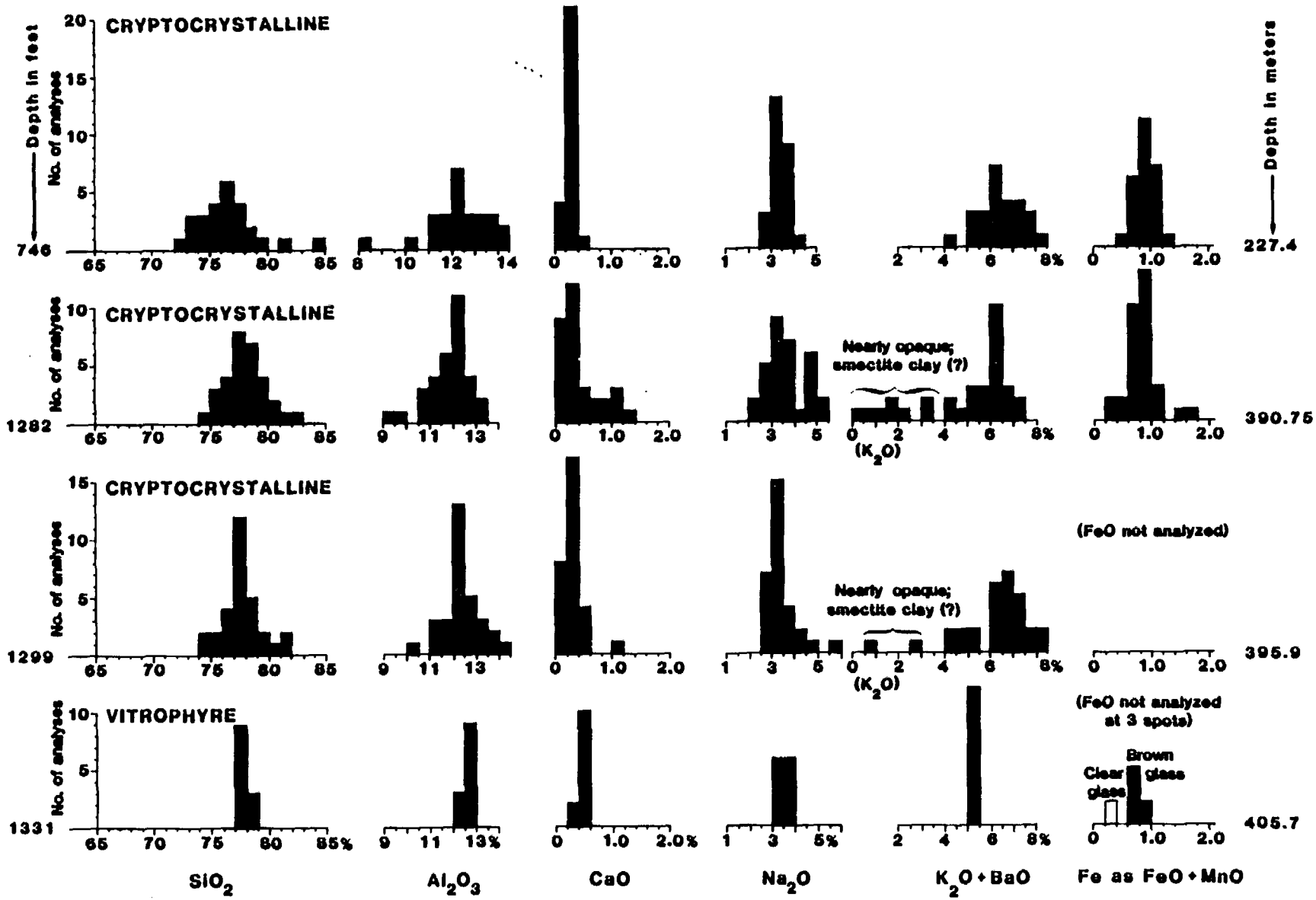

Fig. 7.
Histograms of principal oxides in glassy and very fine grained (cryptocrystalline) matrices of lower part of Topopah Spring Member, USW G-4. Analyses (see Appendix B, Table B-I) normalized to 100% (H_2O and volatile free); analyzed by electron beam microprobe, using 20-μm^2 raster.

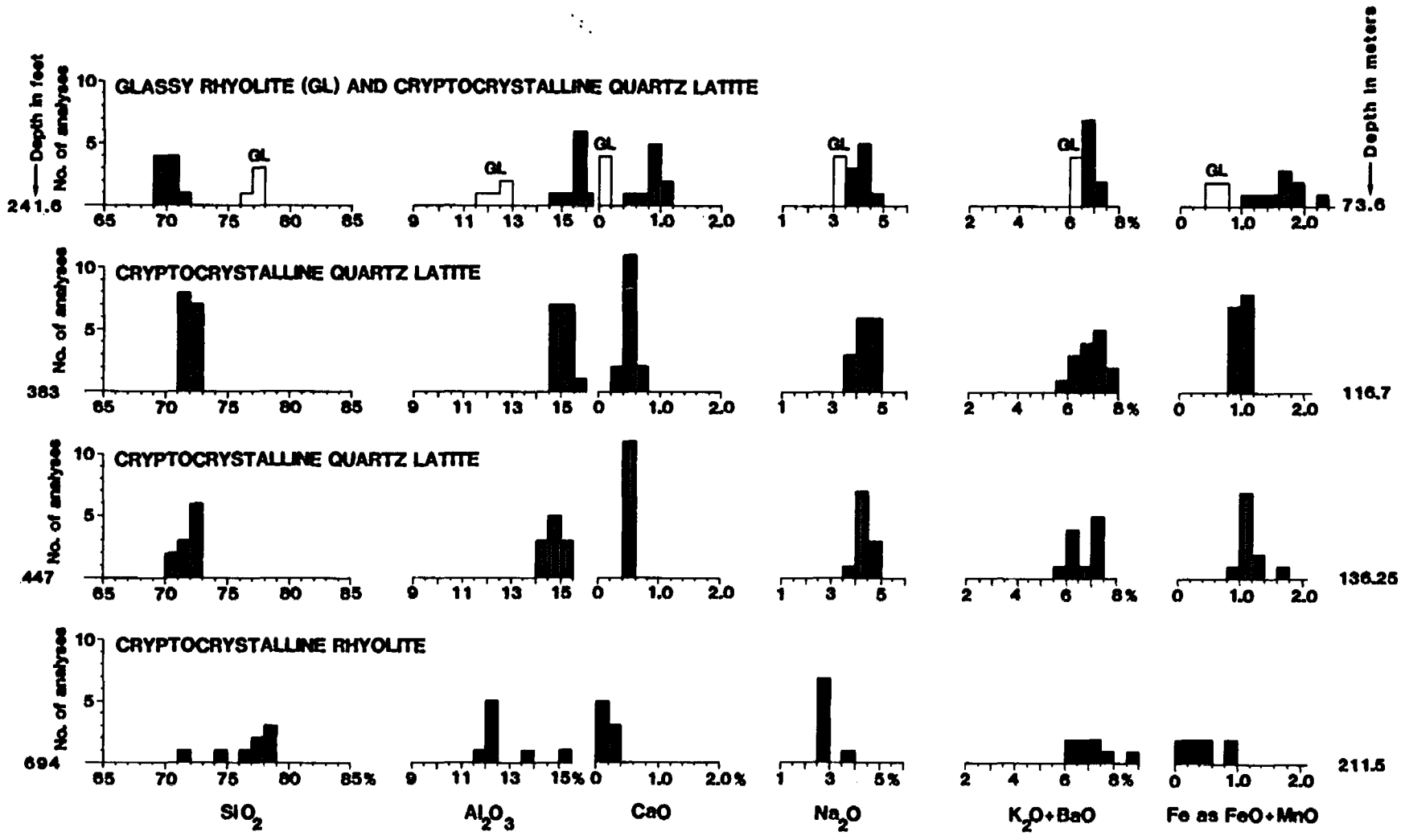

Fig. 8.
Histograms of principal oxides in glassy and very fine grained (cryptocrystalline) matrices of upper part of Topopah Spring Member, USW G-4. Analyses (see Appendix B, Table B-I) normalized to 100% (H_2O and volatile free); analyzed by electron beam microprobe, using 20-μm^2 raster.

447, 383, and 241.6 ft were analyzed by microprobe (Fig. 8; Appendix B, Table B-I). Analyses in the lower two sections at 447 and 383 ft are of cryptocrystalline quartz latite lenticles that differ in composition from the enclosing spherulitic rhyolite and also from the cryptocrystalline high-silica rhyolite of the middle nonlithophysal zone. Clearly the quartz latitic lenticles appear to be magma of different composition, as pointed out by Lipman et al. (1966). The caprock vitrophyre is mostly cryptocrystalline quartz latite except for minor blebs and pumice of clear glass; the composition of this rhyolite is similar to that in the lower three-fourths of the Topopah Spring Member.

IV. DISCUSSION AND CONCLUSIONS

A. Relation of Textures to Emplacement History

In the Topopah Spring matrix, the textural variation with depth is genetically related to cooling and chilling of two major rhyolitic eruptive pulses and an upper gradational zone caused by mixing of a third quartz latitic magma; all erupted about 13 Ma ago (Marvin et al. 1970). The basal vitrophyre and its overlying thick lower nonlithophysal zone (Fig. 2) represent the chilled lower part of the welded ash-flow tuff that was very hot at the time of emplacement (~700°C; Lipman 1971).* The middle nonlithophysal zone is a partially chilled zone that never chilled to a vitrophyre (glass) probably because of a low temperature gradient. The zone's contact with the underlying lower lithophysal zone is gradational, suggesting only a brief hiatus. The upper surface of the lower lithophysal zone was probably still liquid but bubbling with exsolved gases when the second major rhyolitic ash flow erupted. During the cooling and degassing of the second rhyolitic eruptive pulse, the upper lithophysal zone formed above the middle nonlithophysal zone. The upper quartz latitic cryptocrystalline lenticular groundmasses that increase upward are former clots of quartz latitic magma. They accumulated when the lower part of a zoned magma chamber, underlying the Claim Canyon cauldron to the north, was drawn down by the eruption (Lipman et al. 1966; Byers et al. 1976b). This quartz latitic magma, however, has a higher melting point (900°C; Lipman 1971)* than the eruptive temperature of the rhyolitic magma

*Information was also provided by D. E. Broxton, Los Alamos National Laboratory, 1984.

(∿700°C). Therefore, the quartz latitic magma had a greater tendency to chill to a cryptocrystalline groundmass, whereas the rhyolitic magma with its volatiles crystallized to spherulites and granophyre.

The textures in the upper one-fifth of the Topopah Spring illustrate interactions of welding (compaction), crystallization (cooling), and compositional (phenocrysts) zones. From 500.9 ft upward to 383 ft (Fig. 2), the compositional effect is generally one of increasing quartz latitic cryptocrystalline matrix (see Fig. 6b) and phenocrysts; the two trends are not only graphically related but also compositionally related because the increasing crystal assemblage is quartz latitic and includes clinopyroxene. The specimen at 410 ft has a large void and abundant vesicles (pores) indicative of vapor phase action, where part of the quartz latitic matrix crystallized to tiny spherulites 100 to 200 μm in diameter. The thin section at 410 ft was cut close to a large lithophysal cavity. The greatly reduced cryptocrystalline quartz latite in the thin section at 307.6 ft is in the middle of the vapor phase zone, and more than half of the quartz latite matrix has recrystallized to spherulites. The maximum phenocryst (crystal) content of 15.7% at 307.6 ft is related to original crystal content of the quartz latitic magma and the degree of welding (compaction). Microscopically, the upper vitrophyre is mostly very finely cryptocrystalline quartz latite, chilled near the upper surface of the ash flow; only a small amount of colorless rhyolitic glass remains.

In USW G-4, the variation of phenocryst (crystal) proportions with depth (Fig. 2) is related inversely to its original proportions with depth in the magma chamber before eruption. That the phenocrysts precipitated at depth and not at the surface is demonstrated by essentially the same phenocryst assemblage in the basal vitrophyre, which is supercooled magmatic glass, as in the overlying microcrystalline groundmasses including spherulites and granophyre. The phenocryst crystals did not grow after eruption of the Topopah Spring at the surface as did those of the granophyre; rather, they grew at depth before eruption from the magma chamber. The succession of phenocryst assemblages upward from the basal vitrophyre was originally the succession of phenocrysts downward from the top of the magma chamber (Lipman et al. 1966) before eruption.

The small (≲1-mm) quartz phenocrysts are characteristic of the first eruptive pulse, represented from the basal vitrophyre to the top of the lower

lithophysal zone, and were present in the upper part of the magma chamber before eruption. Inasmuch as the phenocrysts constitute only about 1% of the rock, the quartz is exceedingly sparse, even though a few small phenocrysts are seen in every thin section that sampled the first eruptive pulse. Had there been no further magma erupted, the Topopah Spring would be characterized as a high-silica quartz-bearing rhyolite, like the underlying tuffs of Calico Hills. The rhyolite lavas of Calico Hills form an arc of exposures around the Claim Canyon cauldron segment from whence the Topopah Spring Member came (Byers et al. 1976a). The Calico Hills lavas are petrologically similar to the overlying basal tuff of the Topopah Spring and the feldspars of these units show a continuum in composition upward through them (Warren et al. 1984). In fact, studies currently in progress indicate that Crater Flat, Calico Hills, and Paintbrush and Timber Mountain tuffs are all successive eruptive products from the same magmatic hearth (Scott et al. 1984; Warren and Byers 1985; Broxton et al. 1985). However, the volume of ash-flow tuffs of the Crater Flat and Calico Hills is relatively minor compared with that of the Topopah Spring. In other words, by tapping deep into the magma chamber, the eruptive products of the Topopah Spring not only siphoned off the quartz-bearing rhyolitic top but tapped quartz-free crystal-rich quartz-latitic magma at significantly greater depth.

B. Use of Textures to Guide Drilling in Exploratory Shaft

From petrographic study of USW G-4 (Fig. 2), the following preliminary distinctions are suggested, which are based on matrix stratigraphy within the Topopah Spring at the ES site.

1. The lower nonlithophysal zone (candidate host rock) can be distinguished microscopically from the middle nonlithophysal zone by three criteria. First, the lower nonlithophysal zone contains 1.5 to 3.2% foreign lithic fragments (xenoliths), whereas the middle nonlithophysal zone has virtually none. This is understandable because the earlier pulse of the Topopah Spring eruption would be expected to contain more foreign fragments from both the vent walls and the ground surface over which it traveled. Also, indications are that a few lenticular spherulitic pumices in the middle nonlithophysal zone were possibly flattened former lithics that were heated near their melting point and recrystallized. Second, quartz phenocrysts are common in the lower nonlithophysal zone but nearly absent in the

middle nonlithophysal zone. Finally and most significantly, the greater molten lithostatic load at the time of eruption compacted the shards and pumice of the lower nonlithophysal zone into a densely welded tuff, compared with only moderately welded tuff in the middle nonlithophysal zone (Fig. 4).

2. The middle nonlithophysal zone was chilled, as indicated by increased cryptocrystallinity toward the lower contact (Fig. 2); but it was not strongly chilled by a temperature gradient high enough to form a medial vitrophyre, which is found in some thick ash-flow tuffs.
3. The vertical stratigraphic position within each of the two nonlithophysal zones of the Topopah Spring can be estimated by the percentage of cryptocrystalline groundmass (Fig. 2; Appendix A, Table A-I) in a thin section from a sample of core or tunnel wall. The percentage of cryptocrystalline groundmass is inversely related to stratigraphic position above the base of each unit; in other words, the lower the percentage of cryptocrystalline groundmass, the higher the stratigraphic position above the chilled base. This may be a relatively useful stratigraphic criterion: If a horizontal drill hole or tunnel in either of the nonlithophysal zones were to cross a fault (as indicated by lost circulation or gouge), the relative percentages of cryptocrystalline groundmass would indicate which side of the fault was upthrown relative to the other; the lesser cryptocrystalline groundmass would indicate the downthrown side (stratigraphically higher) of the fault. These criteria hold for the lower nonlithophysal zone in drill holes other than USW G-4 (e.g., USW G-1 and GU-3), but the middle nonlithophysal appears thinner in both G-1 and GU-3. Fewer samples are available from these other drill holes, however, and further sampling of the Topopah Spring Member in both of these holes is necessary.
4. The upper lithophysal zone can, in general, be petrographically distinguished from the lower lithophysal zone. The petrographic data indicate only one-third to one-half as many silica-filled vesicles (amygdules) in the lower lithophysal zone compared with the number found in the upper lithophysal zone. These petrographic studies corroborate USGS (Spengler and Chornack 1984) observations that significantly fewer voids occur in the lower lithophysal zone than in

the upper. Cavities in the upper lithophysal zone are also commonly lined with wedge-shaped tridymite crystals (Fig. 6a; Bish et al. 1984) rather than cristobalite.

5. Petrography cannot determine stratigraphic position within lithophysal zones as well as it can determine position within non-lithophysal zones. However, an increase in total phenocrysts and the occurrence of cryptocrystalline quartz latite lenticles (Fig. 6b) within the upper one-third of the upper lithophysal zone (Fig. 2) can, to some extent, indicate stratigraphic position within the zone. Increasing granophyre (Fig. 3a) and larger spherulites (signifying strong vapor-phase action) suggest stratigraphic position within the upper part of the lower lithophysal zone.

The textural differences within the Topopah Spring Member defined by petrochemical study suggest that measurable physical properties might also show systematic variations related to the different textures. Tests to determine the limits of any functional differences between the different matrices should be considered. Such tests might include thermal conductivity, gas permeability, sorption/precipitation, dynamic transport processes, applied diffusion, shaft-sealing cement reaction, time-dependent mechanical or hydrologic properties (e.g., saturation time), and creep tests. At present, some data for the Topopah Spring Member are detailed enough for comparison with the textural categories defined here (e.g., Price et al. 1984), but more such studies are needed.

ACKNOWLEDGMENTS

I thank David Mann for thin section preparation, Roland Hagan and Gary Luedemann for help with electron microprobe analyses and data presentation, and Barbara Hahn for typing the manuscript. Illustrations were drawn by Florence Fujita. Schön Levy took the photomicrographs of definitive textures. D. T. Vaniman, R. G. Warren, and Katherine Campbell reviewed the manuscript.

REFERENCES

Bence, A. E., and A. L. Albee, "Empirical Correction Factors for Electron Microanalysis of Silicates and Oxides," J. Geol., v. 76, 382-403 (1968).

Bish, D. L., F. A. Caporuscio, J. F. Copp, B. M. Crowe, J. D. Purson, J. R. Smyth, and R. G. Warren, "Preliminary Stratigraphic and Petrologic Characterization of Core Samples from USW-G1, Yucca Mountain, Nevada," A. C. Waters and P. R. Carroll, Eds., Los Alamos National Laboratory report LA-8840-MS (1981).

Bish, David L., Allen E. Ogard, David T. Vaniman, and Larry Benson, "Mineralogy-Petrology and Groundwater Geochemistry of Yucca Mountain Tuffs," in Scientific Basis for Nuclear Waste Management VII (Ed. Gary L. McVay), Materials Res. Soc. Symposia Proc., v. 26, North-Holland, New York, 283-291 (1984).

Broxton, D. E., F. M. Byers, Jr., R. G. Warren, and R. B. Scott, "Trends in Phenocryst Chemistry in the Timber Mountain-Oasis Valley Volcanic Field, SW Nevada: Evidence for Episodic Injection of Primitive Magma into an Evolving Magma System," Geol. Soc. America, Abstracts with Programs 1985, v. 17, no. 6, p. 345 (1985).

Byers, F. M., Jr., W. J. Carr, R. L. Christiansen, P. W. Lipman, Paul P. Orkild, and W. D. Quinlivan, "Geologic Map of the Timber Mountain Caldera Area," U.S. Geol. Survey Misc. Geol. Inv. Map I-891 (1976a).

Byers, F. M., Jr., W. J. Carr, Paul P. Orkild, W. D. Quinlivan, and K. A. Sargent, "Volcanic Suites and Related Cauldrons of Timber Mountain-Oasis Valley Caldera Complex, Southern Nevada," U.S. Geol. Surv. Prof. Paper 919, 70 p. (1976b).

Caporuscio, F., D. Vaniman, D. Bish, D. Broxton, B. Arney, G. Heiken, F. Byers, R. Gooley, and E. Semarge, "Petrologic Studies of Drill Cores USW-G2 and UE25b-1H, Yucca Mountain, Nevada," Los Alamos National Laboratory report LA-9255-MS (1982).

Carlos, B. A., "Minerals in Fractures of the Unsaturated Zone from Drill Core USW G-4, Yucca Mountain, Nye County, Nevada," Los Alamos National Laboratory report LA-10415-MS (1985).

Levy, S. S., "Studies of Altered Vitrophyre for the Prediction of Nuclear Waste Repository-Induced Thermal Alteration at Yucca Mountain, Nevada," in Scientific Basis for Nuclear Waste Management VII (Gary L. McVay, Ed.), Materials Res. Soc. Symposia Proc., v.26, North-Holland, New York, 959-966 (1984a).

Levy, S. S., "Petrology of Samples from Drill Holes USW H-3, H-4, and H-5, Yucca Mountain, Nevada," Los Alamos National Laboratory report LA-9706-MS (1984b).

Levy, S. S., "Episodic Zeolitization of Silicic Volcanic Tuff at Yucca Mountain, Nye County, Nevada," Geol. Soc. America, Abstracts with Programs 1985, v. 17, no. 6, p. 366 (1985).

Lipman, P. W., R. L. Christiansen, and J. T. O'Connor, "A Compositionally Zoned Ash-Flow Sheet in Southern Nevada," U.S. Geol. Survey Prof. Paper 524-F, F1-F47 (1966).

Lipman, P. W., "Iron-Titanium Oxide Phenocrysts in Compositionally Zoned Ash-Flow Sheets from Southern Nevada," Jour. Geol., v. 79, 438-456 (1971).

Maldonado, F., and S. L. Koether, "Stratigraphy, Structure and Some Petrographic Features of Tertiary Volcanic Rocks at the USW G-2 Drill Hole, Yucca Mountain, Nye County, Nevada," U.S. Geol. Surv. Open-File Report 83-732, 83 p. (1983).

Marvin, R. F., F. M. Byers, Jr., H. H. Mehnert, P. P. Orkild, and T. W. Stern, "Radiometric Ages and Stratigraphic Sequence of Volcanic and Plutonic Rocks, Southern Nye and Western Lincoln Counties, Nevada," Geol. Soc. Am. Bull., v. 81, 2657-2676 (1970).

Myers, C. W. et al. (Exploratory Shaft Test Plan Committee), "Test Plan for Exploratory Shaft at Yucca Mountain," U.S. Dept. of Energy Nevada Operations Office (Las Vegas, Nevada) Report NVO-244, Revision 0 (November 28, 1983).

Price, R. H., S. J. Spence, and A. K. Jones, "Uniaxial Compression Test Series on Topopah Spring Tuff from USW GU-3, Yucca Mountain, Southern Nevada," Sandia National Laboratories Rept. SAND83-1646 (1984).

Scott, R. B., and Mayra Castellanos, "Preliminary Report on the Geologic Character of Drill Holes USW GU-3 and USW G-3," U.S. Geol. Survey Open-File Report 84-491 (1984).

Scott, R. B., and Jerry Bonk, "Preliminary Geologic Map of Yucca Mountain, Nye County, Nevada, with Geologic Sections," U.S. Geol. Survey Open-File Report 84-494 (1984).

Scott, R. B., F. M. Byers, and R. G. Warren, "Evolution of Magma Below Clustered Calderas, Southwest Nevada Volcanic Field," Trans. Amer. Geophys. Union (EOS), v. 65, no. 45, 1126-1127 (1984).

Smith, R. L., "Zones and Zonal Variations in Welded Ash Flows," U.S. Geol. Survey Prof. Paper 354-F, 149-159 (1960).

Spengler, R. W., D. C. Muller, and R. B. Livermore, "Preliminary Report on the Geology and Geophysics of Drill Hole UE25a-1, Yucca Mountain, Nevada Test Site," U.S. Geol. Surv. Open-File Report 79-1244, 43 p. (1979).

Spengler, R. W., F. M. Byers, Jr., and J. B. Warner, "Stratigraphy and Structure of Volcanic Rocks in Drill Hole USW G-1, Yucca Mountain, Nye County, Nevada," U.S. Geol. Survey Open-File Report 81-1349, 50 p. (1981).

Spengler, R. W., and M. P. Chornack, "Stratigraphic and Structural Characteristics of Volcanic Rocks in Core Hole USW G-4, Yucca Mountain, Nye County, Nevada," with a Section on "Geophysical Logs," D. C. Muller and J. E. Kibler, U.S. Geol. Survey Open-File Report 84-789, 77 p. (1984).

Warren, R. G., F. M. Byers, Jr., and F. A. Caporuscio, "Petrography and Mineral Chemistry of Units of the Topopah Spring, Calico Hills and Crater Flat Tuffs, and Older Volcanic Units, with Emphasis on Samples from Drill Hole USW G-1, Yucca Mountain, Nevada Test Site," Los Alamos National Laboratory report LA-10003-MS (1984).

Warren, R. G., and F. M. Byers, Jr., "The Petrologic Unit: A Useful Tool in Deciphering a Complex Volcanic Terrane in SW Nevada" (Abstract), Geol. Soc. America, Abstracts with Programs 1985, v. 17, no. 4, p. 270 (1985).

APPENDIX A

PETROGRAPHIC MODAL DATA FOR THIN SECTIONS OF TOPOPAH SPRING MEMBER, USW G-4, YUCCA MOUNTAIN, NEVADA

TABLE A-I

PETROGRAPHIC MODAL DATA AS VOLUME PERCENT FOR POLISHED THIN SECTIONS OF TOPOPAH SPRING MEMBER, USW G-4 (Microscopic grains <0.2 mm of sparse zircon and apatite not counted; no sphene seen in any slide; F. M. Byers, analyst)

Cooling Zone (Quasi-stratigraphic)	Depth of Sample (ft)	(m)	Phenocrysts	Lithic Fragments	Granophyre[a]	Amygdules	Spherulites/ Microlites	Cryptocrystalline	Glass	Voids	Points Counted
Upper vitrophyre	241.6	73.6	12.1	0.9	0.0	0.0	0.0	69.7[c]	15.5	1.8	5229
Vapor phase zone	307.6[d]	93.8	15.7	0.1	1.5	3.0	53.6	22.4[c]	0.0	3.7	5663
Vapor phase zone	383	116.7	12.6	0.1	4.2	3.1	34.0	44.8[c]	0.0	1.2	5037
Upper lithophysal	410	125.0	6.8	0.1	4.0	15.3	57.8	5.2[c]	0.0	10.5	5165
" "	416	126.8	8.5	0.0	0.3	3.2	76.6	11.3[c]	0.0	0.1	5217
" "	447	136.2	2.6	0.1	1.2	5.2	83.2	7.6[c]	0.0	0.0	3144[g]
" "	500.9[d]	152.7	0.7	0.4	1.4	6.1	91.0	0.4	0.0	0.5	6220[g]
" "	514	156.7	1.4	0.0	5.3	7.7	82.0	0.0	0.0	3.5	5672[g]
" "	556	169.5	0.6	0.0	3.0	5.8	81.8	0.0	0.0	8.8	5954[g]
Upper lithophysal	625	190.5	1.4	1.5	5.9	1.8	89.3	0.0	0.0	0.0	5556[g]
" "	625.7[d]	190.7	1.0	0.1	6.8	3.9	88.2	0.0	0.0	0.0	5556[g]
" "	677	206.3	0.6	0.1	1.7	3.3	76.9	17.5	0.0	0.0	5624[g]
Middle nonlithophysal	694	211.5	1.1	0.2	1.3	1.3	32.6	63.5	0.0	0.0	5661[g]
"	746	227.4	0.5	0.1	0.8	1.6	12.3	84.6	0.0	0.0	5629[g]
Lower lithophysal	817	249.0	1.6	0.0	10.0	0.0	87.9	0.0	0.0	0.4	5769[g]
" "	934	284.7	0.9	0.6	2.8	2.7	93.1	0.0	0.0	0.0	5936[g]
" "	1026	312.7	0.9	1.3	4.2	1.9	91.5	0.0	0.0	0.2	5402[g]
" "	1089	331.9	0.4	0.6	3.0	2.1	93.8	0.0	0.0	0.0	5897[g]
" "	1117	340.5	1.2	1.9	2.3	1.4	92.9	0.1	0.0	0.1	5409[g]
Lower nonlithophysal	1190	362.7	1.4	1.2	4.7	1.1	78.9	12.6	0.0	0.2	4897[g]
" "	1244	379.2	1.4	2.6	3.8	1.2	51.8	39.1	0.0	0.0	5125[g]
" "	1282	390.8	1.7	1.4	3.4	0.0	26.5	66.8	0.0	0.1	5117[g]
Altered vitrophyre	1299	395.9	1.0	3.2	0.8	0.2[h]	17.5	77.0	0.0	0.3	4960[g]
" "	1311	399.6	1.1	3.1	1.4	0.3[h]	19.7[i]	74.4	0.0	0.0	4971[g]
Lower vitrophyre	1331	405.7	1.0	1.9	0.0	0.0	0.0	0.0	97.0	0.0	10133

[a] Includes microveinlets of silica mineral and feldspar.
[b] Includes anorthoclase.
[c] Cryptocrystalline quartz latite by microprobe analysis.
[d] USGS glass-covered thin section.
[e] Includes 0.6% clinopyroxene, 0.3% hornblende, and 0.2% perrierite.
[f] Includes 0.7% oxyhornblende, 1.1% clinopyroxene, and sparse perrierite(?).
[g] Points counted for phenocryst percentages are approximately double those tabulated.
h Heulandite/clinoptilolite; minor cristobalite.
i Includes about 10% very fine grained smectite clay.
[j] Includes 1.9% hornblende and 0.9% allanite.

TABLE A-I (cont)

Cooling Zone (Quasi-Stratigraphic)	Depth of Sample (ft)	Depth of Sample (m)	Phenocrysts as Volume Percent of Total Phenocrysts: Felsic Minerals: Quartz	Sanidine[b]	Plagioclase	Mafics and Accessories: Biotite	Opaque Oxides	Other Mafics and Accessories	Number Phenocryst Points	Remarks: Other Mafics and Accessories
Upper vitrophyre	241.6	73.6	0.2	53.6	31.4	7.1	4.9	2.8	633	Clinopyroxene; rare perrierite(?)
Vapor phase zone	307.6[d]	93.8	0.0	48.1	42.5	7.6	0.9	0.8	891	" " "
Vapor phase zone	383	116.7	0.0	74.6	21.5	0.6	1.9	1.1[e]	634	See footnote e
Upper lithophysal	410	125.0	0.6	67.1	28.0	1.7	1.7	0.9	353	Clinopyroxene; rare perrierite(?)
" "	416	126.8	0.0	61.4	34.5	0.9	1.4	1.8[f]	443	See footnote f
" "	447	136.2	<1	51.0	44.7	3.4	1.0	<1	208	Clinopyroxene; rare perrierite(?)
" "	500.9[d]	152.7	7	13	66	11	2	0	89	Rare perrierite
" "	514	156.7	1	48	44	3	3	1	143	Clinopyroxene
" "	556	169.5	0	20	78	2	0	0	83	
" "	625	190.5	1	47	45	1.5	4	1.5	137	Mafic pseudomorph; clinopyroxene?
" "	625.7[d]	190.7	0	20	69	6	5	0	101	
" "	677	206.3	0	19	64	5	12	<1	77	Allanite
Middle nonlithophysal	694	211.5	1	21	70	7	1	0	120	
" "	746	227.4	<1	31	61	2	6	0	52	
Lower lithophysal	817	249.0	3	20	71	1	5	0	181	
" "	934	284.7	5	24	67	3	2	0	121	
" "	1026	312.7	9	24	59	6	2	<1	80	Allanite
" "	1089	331.9	6	20	61	6	7	<1	70	"
" "	1117	340.5	1	30	58	5	6	<1	136	"
Lower nonlithophysal	1190	362.7	11	29.5	58	0	1.5	<1	122	"
" "	1244	379.2	23	15	48	7	3	4	122	"
" "	1282	390.8	0.5	32.5	61	1	5	<1	172	"
" "	1299	395.9	5	19	70	3	3	<1	104	"
" "	1311	399.6	12	20	64	3	1	0	110	"
Lower vitrophyre	1331	405.7	16	34	42	5	1	3[j]	108	See footnote j

[a] Includes microveinlets of silica mineral and feldspar.

[b] Includes anorthoclase.

[c] Cryptocrystalline quartz latite by microprobe analysis.

[d] USGS glass-covered thin section.

[e] Includes 0.6% clinopyroxene, 0.3% hornblende, and 0.2% perrierite.

[f] Includes 0.7% oxyhornblende, 1.1% clinopyroxene, and sparse perrierite(?).

[g] Points counted for phenocryst percentages are approximately double those tabulated.

h Heulandite/clinoptilolite; minor cristobalite.

i Includes about 10% very fine-grained smectite clay.

[j] Includes 1.9% hornblende and 0.9% allanite.

APPENDIX B

ELECTRON MICROPROBE ANALYSES OF GROUNDMASSES, TOPOPAH SPRING MEMBER, USW G-4, YUCCA MOUNTAIN, NEVADA

TABLE B-I

ELECTRON MICROPROBE ANALYSES OF GROUNDMASSES, TOPOPAH SPRING MEMBER, USW G-4
YUCCA MOUNTAIN, NEVADA

(Number following G-4 is depth)
(BR--, etc., is sample number of probed area)

SiO2	TiO2	AL2O3	FeO	MgO	CaO	BaO	Na2O	K2O	MnO	TOTAL
TITLE=G4-241.6 CRYPTOCRYSTALLINE (BBR) & GLASSY (GL) GROUNDMASSES										
FILE#64 PT#!23 G4-241.6 BBR4A										
65.83	0.32	15.34	1.64	0.38	0.91	0.25	4.06	6.08	0.22	95.04
FILE#64 PT#!25 G4-241.6 BBR4C										
66.63	0.34	15.20	1.55	0.25	0.86	0.18	3.63	6.63	0.19	95.47
FILE#64 PT#!26 G4-241.6 BBR4D										
66.65	0.31	15.21	1.05	0.39	1.09	0.05	4.04	6.18	0.37	95.34
FILE#64 PT#!28 G4-241.6 BBR5B										
66.75	0.36	15.07	1.51	0.26	0.77	0.16	4.16	6.21	0.11	95.36
FILE#64 PT#!29 G4-241.6 BBR5C										
66.05	0.34	15.03	0.95	0.35	1.06	0.18	3.73	6.47	0.18	94.33
FILE#64 PT#!31 G4-241.6 BBR3A										
66.14	0.34	14.54	1.94	0.30	0.86	0.00	3.42	6.43	0.17	94.13
FILE#64 PT#!32 G4-241.6 BBR2A										
67.25	0.36	15.14	0.93	0.12	0.63	0.14	4.18	6.15	0.14	95.04
FILE#64 PT#!35 G4-241.6 GL1A										
73.38	0.06	11.20	0.35	0.01	0.13	0.12	3.08	5.90	0.03	94.25
FILE#64 PT#!36 G4-241.6 GLP1A (glassy pumice)										
73.02	0.03	11.88	0.58	0.00	0.15	0.00	3.19	5.85	0.09	94.79
FILE#64 PT#!37 G4-241.6 GL2A										
72.84	0.04	11.96	0.47	0.00	0.15	0.09	3.27	5.90	0.00	94.72
FILE#64 PT#!38 G4-241.6 BBR7A										
65.82	0.38	14.97	1.41	0.31	0.87	0.17	4.32	6.16	0.18	94.60
FILE#64 PT#!39 G4-241.6 BBR9A										
68.14	0.27	14.06	1.38	0.14	0.54	0.09	4.28	6.37	0.20	95.46
FILE#64 PT#!41 G4-241.6 GL5A										
73.33	0.10	11.73	0.71	0.03	0.17	0.10	2.84	5.77	0.02	94.79
TITLE=G4-383 BROWN CRYPTOCRYSTALLINE GROUNDMASS										
FILE#53 PT#6 G4-383 BR1A										
70.71	0.32	15.01	1.12	0.00	0.39	0.24	4.37	6.89	0.05	99.09
FILE#53 PT#9 G4-383 BR1C										
72.39	0.28	15.19	0.78	0.02	0.43	0.00	4.21	6.98	0.07	100.35
FILE#53 PT#10 G4-383 BR1D										
72.87	0.28	15.06	0.96	0.01	0.48	0.11	4.60	6.44	0.09	100.90
FILE#53 PT#11 G4-383 BR1E										
72.57	0.26	15.03	1.08	0.03	0.49	0.00	4.06	7.25	0.08	100.85
FILE#53 PT#12 G4-383 BR2A (different area)										
71.63	0.26	14.72	1.11	0.01	0.37	0.01	3.84	7.57	0.05	99.56
FILE#53 PT#13 G4-383 BR2B										
70.24	0.25	15.10	0.81	0.00	0.38	0.00	3.68	7.86	0.00	98.31
FILE#53 PT#15 G4-383 BR2C										
70.46	0.24	15.02	0.98	0.00	0.59	0.01	4.64	6.29	0.08	98.31

TABLE B-I (cont)

SiO2	TiO2	AL2O3	FeO	MgO	CaO	BaO	Na2O	K2O	MnO	TOTAL
FILE#53 PT#16 G4-383 BR2D										
71.02	0.30	14.99	0.91	0.10	0.54	0.00	3.96	7.39	0.03	99.24
FILE#53 PT#17 G4-383 BR3A (different area)										
71.47	0.32	15.02	0.95	0.05	0.60	0.18	4.77	5.76	0.03	99.15
FILE#53 PT#18 G4-383 BR3B										
70.32	0.31	15.04	0.96	0.02	0.50	0.00	4.51	6.67	0.02	98.36
FILE#53 PT#19 G4-383 BR3C										
71.90	0.29	14.42	0.91	0.01	0.42	0.10	4.37	6.62	0.06	99.11
FILE#53 PT#20 G4-383 BR3D										
71.47	0.29	14.36	0.97	0.03	0.57	0.00	4.82	6.02	0.06	98.59
FILE#53 PT#21 G4-383 BR3E										
70.83	0.31	15.48	1.16	0.03	0.51	0.10	4.82	6.48	0.00	99.72
FILE#53 PT#22 G4-383 BR3F										
72.25	0.31	14.91	0.86	0.02	0.41	0.17	4.16	6.89	0.00	99.99
FILE#53 PT#23 G4-383 BR3G										
71.78	0.26	14.89	0.93	0.00	0.42	0.19	4.29	6.88	0.00	99.64
TITLE=G4-447 BROWN CRYPTOCRYSTALLINE GROUNDMASS										
FILE#53 PT#!82 G4-447 BR1A										
72.10	0.33	14.79	1.18	0.15	0.50	0.23	4.52	6.19	0.00	99.98
FILE#54 PT#!85 G4-447 BR1C										
70.45	0.26	15.11	1.23	0.19	0.54	0.15	4.44	6.66	0.09	99.12
FILE#54 PT#!86 G4-447 BR1D										
71.15	0.29	14.79	1.10	0.17	0.48	0.12	4.21	7.08	0.00	99.41
FILE#54 PT#!91 G4-447 BR1G										
69.89	0.36	14.91	1.25	0.24	0.41	0.17	4.24	6.67	0.38	98.63
FILE#54 PT#!92 G4-447 BR2A (different area)										
69.82	0.26	14.70	0.97	0.07	0.46	0.09	4.03	6.89	0.13	97.42
FILE#54 PT#!93 G4-447 BR2B										
73.41	0.22	14.56	0.87	0.07	0.48	0.00	3.69	7.39	0.11	100.81
FILE#54 PT#!94 G4-447 BR2C										
73.27	0.27	14.62	1.11	0.08	0.45	0.08	4.11	6.35	0.19	100.54
FILE#54 PT#!95 G4-447 BR2D										
73.83	0.21	14.66	0.91	0.11	0.47	0.00	4.44	6.44	0.14	101.20
FILE#54 PT#!96 G4-447 BR2E										
73.77	0.30	14.91	1.11	0.09	0.43	0.04	4.67	5.83	0.09	101.22
FILE#54 PT#!97 G4-447 BR2F										
70.74	0.26	14.49	0.90	0.02	0.42	0.07	4.57	6.28	0.19	97.95
FILE#54 PT#!98 G4-447 BR2G										
70.55	0.23	14.07	0.96	0.05	0.42	0.12	4.10	6.87	0.18	97.55
TITLE=G4-694 BROWN CRYPTOCRYSTALLINE GROUNDMASS										
FILE#55 PT# 4 G4-694 BR2A										
77.11	0.04	12.15	0.79	0.03	0.20	0.91	2.81	6.35	0.06	100.44
FILE#55 PT# 5 G4-694 BR2B										
74.95	0.09	13.79	0.73	0.10	0.21	0.00	2.89	7.79	0.08	100.62
FILE#55 PT# 6 G4-694 BR2C										
77.56	0.04	11.57	0.26	0.02	0.13	0.00	2.68	6.67	0.00	98.92
FILE#55 PT# 7 G4-694 BR2D										
71.20	0.02	15.40	0.24	0.04	0.25	0.00	3.62	8.76	0.00	99.53

TABLE B-I (cont)

SiO2	TiO2	AL2O3	FeO	MgO	CaO	BaO	Na2O	K2O	MnO	TOTAL
FILE#55 PT# 8 G4-694 BR2E										
77.13	0.03	11.97	0.41	0.06	0.16	0.00	2.72	6.56	0.00	99.05
FILE#55 PT# 9 G4-694 BR2F										
78.53	0.00	12.30	0.12	0.00	0.18	0.00	2.89	6.53	0.07	100.61
FILE#55 PT#10 G4-694 BR2G										
78.11	0.04	12.27	0.16	0.00	0.17	0.00	2.68	7.04	0.00	100.48
FILE#55 PT#11 G4-694 BR2H										
78.05	0.05	12.02	0.42	0.03	0.19	0.00	2.97	6.24	0.02	99.99
TITLE=G4-746 BROWN CRYPTOCRYSTALLINE GROUNDMASS										
FILE#45 PT#1 G4-746 BR1A										
72.70	0.13	13.67	0.53	0.18	0.31	0.00	3.81	6.41	0.06	97.81
FILE#45 PT#2 G4-746 BR1B										
72.11	0.12	12.36	0.81	0.21	0.43	0.04	3.67	4.99	0.14	94.86
FILE#45 PT#4 G4-746 BR1C										
79.74	0.07	11.05	0.65	0.03	0.28	0.00	3.12	5.02	0.05	100.00
FILE#45 PT#5 G4-746 BR1D										
74.84	0.08	10.46	0.79	0.05	0.21	0.00	2.71	5.72	0.11	94.97
FILE#45 PT#6 G4-746 BR1E										
72.63	0.08	14.20	0.64	0.02	0.31	0.00	4.26	7.22	0.00	99.38
FILE#45 PT#7 G4-746 BR1F										
75.84	0.10	12.46	1.27	0.10	0.34	0.00	3.56	6.21	0.07	99.93
FILE#45 PT#8 G4-746 BR1G										
77.70	0.09	11.95	0.81	0.03	0.22	0.00	3.24	6.43	0.08	100.55
FILE#45 PT#9 G4-746 BR1H										
74.82	0.11	12.74	0.89	0.04	0.12	0.00	3.11	7.35	0.06	99.24
FILE#45 PT#10 G4-746 BR1J										
73.41	0.11	12.66	0.78	0.05	0.16	0.02	3.23	7.38	0.08	97.88
FILE#45 PT#11 G4-746 BR1K										
74.19	0.08	12.62	0.85	0.11	0.25	0.00	3.34	6.61	0.17	98.23
FILE#45 PT#12 G4-746 BR1L										
72.68	0.09	14.43	0.88	0.00	0.22	0.12	3.79	7.74	0.15	100.10
FILE#45 PT#13 G4-746 BR1M										
77.74	0.06	11.78	0.73	0.00	0.27	0.05	3.75	5.50	0.13	100.01
FILE#45 PT#14 G4-746 BR2A (new area)										
78.36	0.09	11.30	0.84	0.03	0.22	0.09	3.17	5.72	0.10	99.93
FILE#45 PT#15 G4-746 BR2B										
74.31	0.09	13.41	0.77	0.05	0.23	0.00	3.82	7.11	0.25	100.04
FILE#45 PT#16 G4-746 BR2C										
76.84	0.05	12.45	0.76	0.00	0.22	0.14	3.45	6.30	0.13	100.33
FILE#45 PT#17 G4-746 BR3A										
73.61	0.00	13.02	0.46	0.00	0.27	0.00	3.41	7.38	0.06	98.21
FILE#45 PT#18 G4-746 BR3B										
82.89	0.05	8.08	0.54	0.01	0.19	0.03	2.55	4.09	0.11	98.53
FILE#45 PT#19 G4-746 BR3C										
77.21	0.06	11.69	0.83	0.02	0.25	0.09	3.35	6.02	0.16	99.70
FILE#45 PT#20 G4-746 BR3D										
77.54	0.07	12.17	0.77	0.08	0.31	0.00	3.35	5.97	0.15	100.41
FILE#45 PT#21 G4-746 BR4A										
80.44	0.10	9.91	0.53	0.02	0.29	0.00	2.60	4.98	0.13	99.01

TABLE B-I (cont)

SiO2	TiO2	AL2O3	FeO	MgO	CaO	BaO	Na2O	K2O	MnO	TOTAL
FILE#45 PT#22 G4-746 BR4B										
77.16	0.06	12.12	0.68	0.00	0.20	0.00	3.06	6.77	0.18	100.24
FILE#45 PT#23 G4-746 BR4C										
75.60	0.10	12.36	0.82	0.00	0.24	0.00	3.76	6.06	0.20	99.15
FILE#45 PT#24 G4-746 BR4D										
76.43	0.08	12.22	0.97	0.03	0.17	0.00	3.04	6.71	0.14	99.80
FILE#45 PT#25 G4-746 BR4E										
74.18	0.10	13.85	1.01	0.06	0.18	0.00	3.07	8.20	0.08	100.72
FILE#45 PT!25 G4-746 BR4F										
75.62	0.07	12.14	0.51	0.02	0.24	0.00	3.49	6.34	0.08	98.50
FILE#45 PT!26 G4-746 BR4G										
73.29	0.10	13.71	0.84	0.00	0.23	0.00	3.58	7.32	0.10	99.16
TITLE=G4-1244 SPHERULITIC GROUNDMASS										
FILE#36 PT#6 G4-1244 BR-0 (spherulite)										
77.85	0.11	12.29	0.94	0.03	0.16	0.05	3.07	6.82	0.09	101.42
TITLE=G4-1282 BROWN CRYPTOCRYSTALLINE GROUNDMASS										
FILE#40 PT#!31 G4-1282 BR1A										
79.02	0.06	11.45	0.61	0.05	0.69	0.25	4.62	2.94	0.03	99.73
FILE#40 PT#!33 G4-1282 BR1C										
77.38	0.08	11.73	0.85	0.06	0.20	0.15	3.11	6.09	0.13	99.77
FILE#40 PT#!34 G4-1282 BR1D										
78.34	0.10	11.62	0.80	0.05	0.19	0.02	2.96	6.19	0.13	100.40
FILE#40 PT#!35 G4-1282 BR2A										
77.08	0.11	12.29	0.75	0.07	0.38	0.13	3.37	6.53	0.05	100.75
FILE#40 PT#!36 G4-1282 BR2B										
72.42	0.15	12.58	0.85	0.05	0.19	0.09	3.42	6.88	0.06	96.68
FILE#40 PT#!37 G4-1282 BR2C										
72.99	0.14	12.53	0.91	0.10	0.25	0.08	3.43	6.68	0.07	97.17
FILE#40 PT#!41 G4-1282 BR2D										
76.32	0.12	12.50	0.77	0.00	0.24	0.07	3.06	6.99	0.08	100.14
FILE#40 PT#!42 G4-1282 BR3A										
81.39	0.10	10.04	0.81	0.04	0.24	0.00	2.88	4.97	0.07	100.55
FILE#40 PT#!43 G4-1282 BR3B										
75.00	0.08	12.70	0.57	0.07	0.32	0.06	3.64	6.30	0.03	98.78
FILE#40 PT#!44 G4-1282 BR3C										
77.79	0.07	10.92	0.25	0.02	0.35	0.06	3.53	5.45	0.09	98.53
FILE#47 PT#4 G4-1282 BR4A										
76.25	0.10	12.66	1.48	0.09	1.12	0.00	5.25	1.93	0.06	98.92
FILE#47 PT#5 G4-1282 BR4B										
76.30	0.05	11.54	1.56	0.12	0.88	0.00	4.55	2.05	0.06	97.12
FILE#47 PT#6 G4-1282 BR4C										
77.24	0.02	12.00	0.54	0.08	0.32	0.00	3.17	5.37	0.05	98.79
FILE#47 PT#7 G4-1282 BR4D										
75.71	0.05	13.42	0.72	0.06	0.59	0.00	4.58	4.42	0.00	99.53
FILE#47 PT#8 G4-1282 BR4E										
77.63	0.04	11.80	0.71	0.04	0.19	0.00	3.17	6.03	0.08	99.69
FILE#47 PT#9 G4-1282 BR4F										
77.25	0.06	12.23	0.74	0.08	0.19	0.00	3.02	6.30	0.04	99.90

TABLE B-I (cont)

SiO2	TiO2	AL2O3	FeO	MgO	CaO	BaO	Na2O	K2O	MnO	TOTAL
FILE#47 PT#10 G4-1282 BR4G										
77.50	0.06	12.40	0.74	0.02	0.18	0.00	3.08	6.52	0.07	100.58
FILE#47 PT#11 G4-1282 BR4H										
83.13	0.03	9.32	0.58	0.06	0.17	0.00	2.43	5.05	0.14	100.92
FILE#47 PT#12 G4-1282 BR4J										
74.55	0.07	11.99	0.86	0.10	0.31	0.25	3.29	5.93	0.14	97.49
FILE#47 PT#13 G4-1282 BR5A (different area of slide)										
76.68	0.04	11.94	0.70	0.06	0.40	0.06	3.42	5.17	0.09	98.56
FILE#47 PT#14 G4-1282 BR5B										
77.90	0.06	10.97	0.74	0.03	0.23	0.04	2.80	6.04	0.07	98.88
FILE#47 PT#15 G4-1282 BR5C										
77.17	0.03	11.03	0.46	0.04	0.51	0.02	3.85	4.19	0.18	97.48
FILE#47 PT#16 G4-1282 BR5D										
77.48	0.04	11.68	0.73	0.05	0.17	0.15	2.75	5.83	0.11	98.98
FILE#47 PT#17 G4-1282 BR5E										
77.43	0.04	11.72	0.75	0.02	0.74	0.00	4.17	2.98	0.09	97.94
FILE#47 PT#18 G4-1282 BR5F										
75.37	0.05	11.67	0.69	0.06	0.32	0.00	2.83	6.02	0.13	97.14
FILE#47 PT#19 G4-1282 BR5G										
75.23	0.02	11.52	0.24	0.01	0.09	0.00	2.15	5.86	0.12	95.24
FILE#47 PT#20 G4-1282 BR5H										
81.81	0.05	10.54	0.74	0.02	1.33	0.02	4.81	0.42	0.16	99.90
FILE#47 PT#21 G4-1282 BR5J										
77.58	0.08	11.43	0.90	0.08	1.00	0.02	5.05	1.27	0.00	97.42
FILE#47 PT#22 G4-1282 BR5K										
80.51	0.05	10.79	0.45	0.00	1.04	0.00	4.84	0.75	0.00	98.42
FILE#47 PT#23 G4-1282 BR5L										
80.41	0.11	10.84	1.05	0.09	0.87	0.02	4.80	1.81	0.00	99.99
FILE#47 PT#24 G4-1282 BR5M										
75.30	0.06	12.74	0.57	0.03	0.19	0.09	3.12	7.23	0.00	99.33
FILE#47 PT#25 G4-1282 BR5N										
73.01	0.04	11.68	0.66	0.03	0.23	0.07	3.42	5.60	0.00	94.73
TITLE=G4-1299 BROWN CRYPTOCRYSTALLINE GROUNDMASS (FeO not analyzed)										
FILE#49 PT#7 G4-1299 BR1A										
71.89	0.05	12.80	----	0.00	0.19	0.00	2.54	7.88	0.00	95.35
FILE#49 PT#8 G4-1299 BR1B										
75.83	0.07	11.59	----	0.00	0.19	0.00	2.46	6.76	0.00	96.88
FILE#49 PT#9 G4-1299 BR1C										
74.05	0.05	11.91	----	0.03	0.17	0.00	2.46	7.47	0.00	96.14
FILE#49 PT#10 G4-1299 BR1D										
77.56	0.04	12.20	----	0.00	0.53	0.00	3.35	5.18	0.00	98.87
FILE#49 PT#11 G4-1299 BR1E										
77.10	0.07	12.53	----	0.03	0.19	0.00	3.22	6.59	0.04	99.77
FILE#49 PT#12 G4-1299 BR1F										
76.17	0.05	12.18	----	0.05	0.22	0.00	3.29	6.01	0.03	98.00
FILE#49 PT#13 G4-1299 BR1G										
77.08	0.06	12.21	----	0.04	0.22	0.00	2.79	6.78	0.00	99.18
FILE#49 PT#14 G4-1299 BR1H										
74.83	0.07	12.25	----	0.04	0.29	0.00	3.53	6.01	0.03	97.06

TABLE B-I (cont)

SiO2	TiO2	AL2O3	FeO	MgO	CaO	BaO	Na2O	K2O	MnO	TOTAL
FILE#49 PT#15 G4-1299 BR1J										
76.87	0.06	12.26	----	0.03	0.14	0.00	2.71	7.39	0.05	99.53
FILE#49 PT#16 G4-1299 BR1K										
72.36	0.02	13.41	----	0.07	0.20	0.00	2.75	8.12	0.02	96.95
FILE#49 PT#18 G4-1299 BR1M										
75.94	0.02	11.50	----	0.05	1.06	0.00	5.54	0.51	0.00	94.61
FILE#49 PT#19 G4-1299 BR1N										
74.65	0.05	12.19	----	0.04	0.19	0.00	3.08	7.17	0.02	97.38
FILE#49 PT#20 G4-1299 BR1P										
76.46	0.08	12.09	----	0.05	0.17	0.00	2.98	6.38	0.00	98.20
FILE#49 PT#21 G4-1299 BR1Q										
79.39	0.08	10.13	----	0.04	0.19	0.00	2.97	4.48	0.01	97.30
FILE#49 PT#22 G4-1299 BR2A (new area)										
72.54	0.09	13.98	----	0.06	0.25	0.02	3.28	7.48	0.03	97.73
FILE#49 PT#23 G4-1299 BR2B										
73.15	0.10	12.43	----	0.10	0.24	0.15	2.89	6.46	0.05	95.56
FILE#49 PT#24 G4-1299 BR2C										
78.22	0.10	11.04	----	0.06	0.37	0.14	3.43	4.54	0.00	97.90
FILE#49 PT#25 G4-1299 BR2D										
73.31	0.06	11.77	----	0.04	0.17	0.14	3.06	6.13	0.00	94.67
FILE#49 Pt#!11 G4-1299 BR2E										
74.51	0.10	13.04	----	0.03	0.17	0.00	3.07	7.23	0.02	98.18
FILE#50 PT#!12 G4-1299 BR2F										
72.21	0.08	11.93	----	0.06	0.20	0.15	2.94	6.98	0.09	94.64
FILE#50 PT#!14 G4-1299 BR2H										
76.48	0.14	12.31	----	0.03	0.47	0.05	3.74	5.20	0.02	98.42
FILE#50 PT#!15 G4-1299 BR2J										
76.51	0.10	12.21	----	0.03	0.32	0.15	3.13	6.02	0.00	98.49
FILE#50 PT#!16 G4-1299 BR2K										
78.08	0.12	12.32	----	0.04	0.57	0.06	4.06	4.46	0.03	99.75
FILE#50 PT#!17 G4-1299 BR2L										
76.46	0.09	12.15	----	0.05	0.27	0.21	2.89	6.73	0.00	98.86
FILE#50 PT#!18 G4-1299 BR2M										
78.21	0.12	11.53	----	0.04	0.38	0.07	4.04	4.18	0.00	98.57
FILE#50 PT#!19 G4-1299 BR2N										
75.26	0.10	12.27	----	0.07	0.25	0.17	3.06	6.59	0.00	97.77
FILE#50 PT#!20 G4-1299 BR2P										
79.88	0.11	10.91	----	0.05	0.50	0.24	4.53	2.32	0.04	98.57
FILE#50 PT#!21 G4-1299 BR2Q										
77.01	0.09	11.56	----	0.08	0.24	0.20	3.47	5.98	0.00	98.62
FILE#50 PT#!22 G4-1299 BR2R										
76.42	0.09	11.66	----	0.05	0.20	0.19	3.19	5.90	0.02	97.71
FILE#50 PT#!23 G4-1299 BR2S										
76.52	0.08	12.04	----	0.06	0.23	0.24	3.20	6.33	0.00	98.69
TITLE=G4-1331 VITROPHYRE GLASS (GROUNDMASS) ANALYSES										
FILE#51 PT# 3 G4-1331 BR1A (FeO not analyzed)										
75.00	0.02	11.91	----	0.02	0.46	0.05	3.32	4.94	0.00	95.72
FILE#51 PT# 4 G4-1331 BR1B (FeO not analyzed)										
75.03	0.00	12.03	----	0.05	0.47	0.09	3.36	4.87	0.00	95.81

TABLE B-I (cont)

SiO2	TiO2	AL2O3	FeO	MgO	CaO	BaO	Na2O	K2O	MnO	TOTAL
FILE#51 PT# 7 G4-1331 BR1C (FeO not analyzed)										
73.91	0.07	11.98	----	0.03	0.47	0.04	3.40	4.97	0.00	94.87
FILE#52 PT# 3 G4-1331 BR1D										
73.85	0.04	12.12	0.61	0.02	0.45	0.05	3.39	4.90	0.08	95.51
FILE#52 PT# 6 G4-1331 BR1H										
73.64	0.03	12.02	0.67	0.02	0.41	0.00	3.35	4.88	0.04	95.06
FILE#52 PT#14 G4-1331 BR2C										
75.02	0.03	11.75	0.70	0.00	0.42	0.00	3.26	4.87	0.00	96.05
FILE#52 PT#15 G4-1331 BR2D										
73.76	0.04	12.15	0.64	0.02	0.42	0.03	3.44	4.91	0.00	95.41
FILE#52 PT#16 G4-1331 BR2E										
73.04	0.03	11.92	0.75	0.02	0.43	0.00	3.34	4.85	0.04	94.41
FILE#52 PT#21 G4-1331 BR2G										
74.20	0.12	12.28	0.76	0.01	0.42	0.00	3.21	5.03	0.14	96.17
FILE#52 PT#22 G4-1331 BR2H (colorless glass rim on brown glass)										
74.24	0.11	12.18	0.19	0.00	0.34	0.01	3.33	4.96	0.11	95.47
FILE#52 PT#23 G4-1331 BR2J (same as above)										
73.74	0.10	12.29	0.17	0.00	0.37	0.00	3.31	4.96	0.06	95.00

☆ U.S. Government Printing Office 1985-676-104/20019

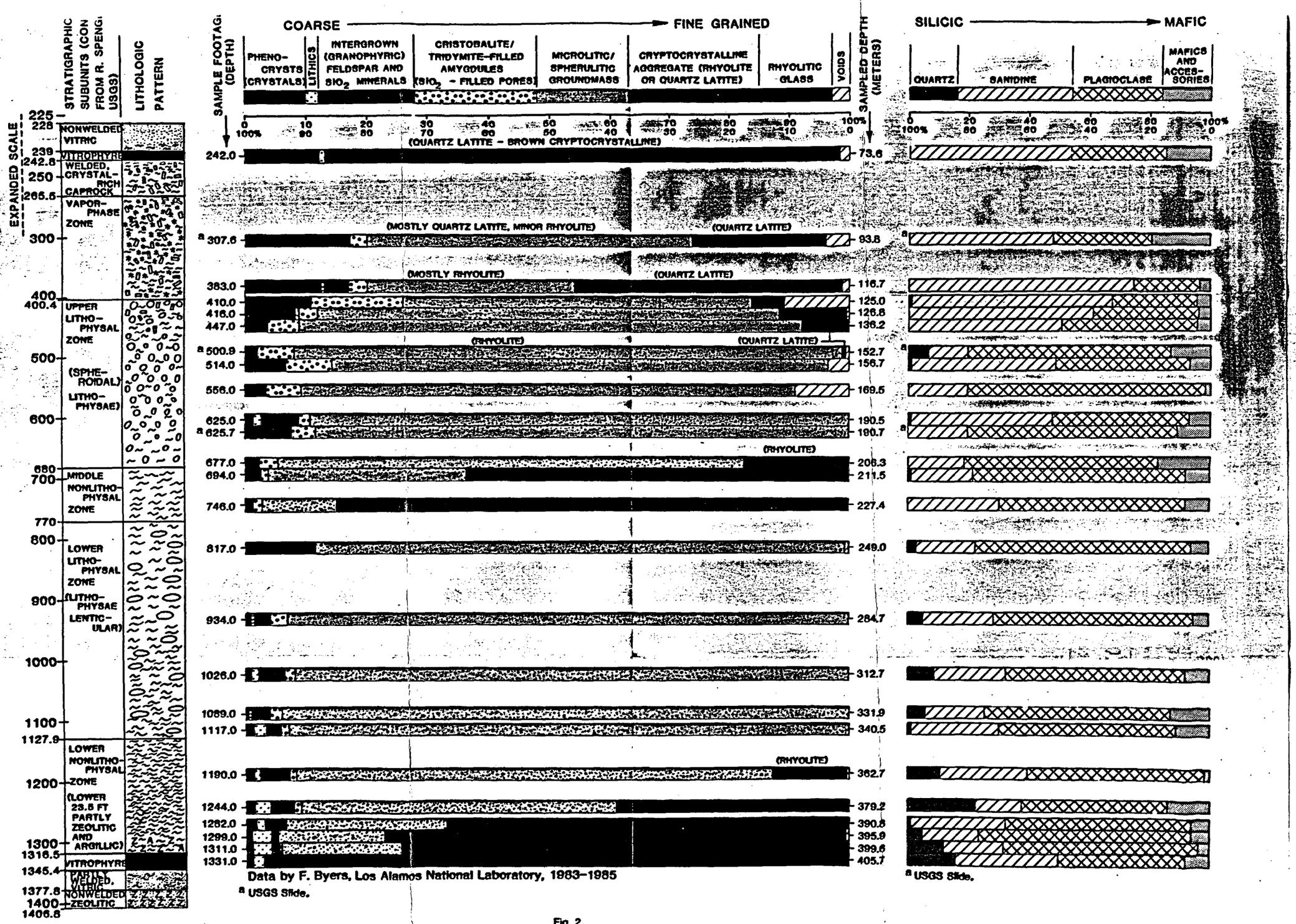

Fig. 2.
Petrographic textural and phenocryst variation of Topopah Spring matrix with depth (stratigraphic position) in drill hole USW G-4, Yucca Mountain. Contacts in stratigraphic column from Spengler et al. (1984)

Los Alamos